Molecular Junctions of Self-Assembled Monolayers with Conducting Polymer Contacts

Alexander B. Neuhausen, Ali Hosseini, Joseph A. Sulpizio, Christopher E. D. Chidsey, and David Goldhaber-Gordon*

Stanford University, Stanford, California 94305, United States

ABSTRACT

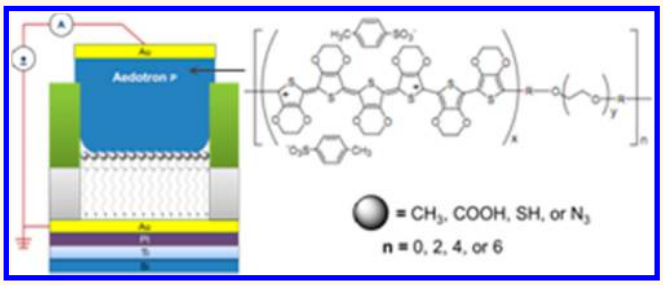

We present a method to fabricate individually addressable junctions of self-assembled monolayers (SAMs) that builds on previous studies which have shown that soft conductive polymer top contacts virtually eliminate shorts through the SAMs. We demonstrate devices with nanoscale lateral dimensions, representing an order of magnitude reduction in device area, with high yield and relatively low device-to-device variation, improving several features of previous soft contact devices. The devices are formed in pores in an inorganic dielectric layer with features defined by e-beam lithography and dry etching. We replace the aqueous PEDOT:PSS conductive polymer used in prior devices with Aedotron P, a low-viscosity, amphiphilic polymer, allowing incorporation of self-assembled monolayers with either hydrophobic or hydrophilic termination with the same junction geometry and materials. We demonstrate the adaptability of this new design by presenting transport measurements on SAMs composed of alkanethiols with methyl, thiol, carboxyl, and azide terminations. We establish that the observed room-temperature tunnel barrier is primarily a function of monolayer thickness, independent of the terminal group's hydrophilicity. Finally, we investigate the temperature dependence of transport and show that the low-temperature behavior is based on the energy distribution of sites from which carriers can tunnel between the polymer and gold contacts, as described by a model of variable-range hopping transport in a disordered conductor.

KEYWORDS: molecular electronics · self-assembled monolayer · transport · alkanethiol · conductive polymer · variable-range hopping

Molecular-scale electronics promises a means to achieve device dimensions smaller than those allowed by the physical limitations of semiconductor materials, potentially enabling extremely scaled processing and memory elements for use in more powerful, lower-energy-consuming computers and information storage units.[1−3] Numerous device designs utilizing single or few organic molecules have been proposed, ranging from simple two-terminal memory elements to complex multi-input and output logic elements.[4−6] Investigations of molecular transport can be considered in two broad categories. The first category focuses on the statistical distribution of measurements of two-terminal single-molecule structures, typically employing contact geometries that could not be readily integrated into a scalable architecture. The methods used for these types of experiments include the probing of molecules on substrates as in scanning tunneling microscopy and conducting atomic force microscopy, as well as the measurement of molecules spanning narrow junctions formed from wires broken by electromigration or electromechanical strain.[7,8] The second category is concerned with parallel transport through many molecules in a SAM.[9−27] In contrast to single-molecule experiments, many SAM-based measurements are designed with the goal of fabricating scalable devices with low variation. This is the challenge addressed by the present work.

As detailed by Akkerman *et al.*, a molecular electronics device should sandwich the molecules between two electrodes and utilize the ordered molecular domains of a SAM to ensure low variation and consistent physical properties as the device footprint is scaled.[9] A variety of fabrication methods with this geometry have been explored in previous work, but each one suffers from either low yield due to shorting, drawbacks associated with the use of photoresist as a dielectric material, or limitations from the need to use molecular terminations that are compatible with the top contact.

Most proposed molecular electronics devices incorporating SAMs are benchmarked with transport measurements of an alkanethiol SAM assembled on a gold substrate

* Address correspondence to goldhaber-gordon@stanford.edu.

Received for review August 3, 2012 and accepted October 4, 2012.

Published online 10.1021/nn3035183

because of the fast and robust monolayer formation in this system. The first such devices employed simple vapor deposition of metal contacts onto SAMs in pores fabricated in a thin dielectric layer.[10,11,17,18] This technique allows fabrication of devices at a scale of tens of nanometers. However, metal filament formation in the monolayer produces poor yield when the SAM consists of any molecules other than alkanedithiols[12] or the evaporated contact is formed from any material other than gold.[13] A more recent technique by Preiner *et al.* utilizes atomic layer deposition (ALD) to deposit an initial barrier of a few atomic layers of insulating material upon which metal contacts can be deposited without forming shorts.[14] Even a thin layer of ALD-deposited alumina is resistant to evaporated metal diffusion, and the initial atomic layers of the alumina preferentially deposit at defect sites in the SAM, passivating the areas most prone to shorting. This procedure has thus far been limited to molecules with hydrophilic terminations, as the water vapor used in ALD of alumina will not wet a hydrophobic monolayer. Alternatively, methods based on pattern transfer of a metallic contact, prefabricated on another substrate, onto the top of a SAM allow for the use of any molecular termination for the SAM. One such method, lift-on lithography, is limited to relatively large, continuous structures.[15] Nanoimprint lithography enables application of high-resolution top contacts but appears to suffer from limited durability, as the SAM residing between the contacts is not confined to a rigid structure.[16] Finally, a variety of devices have been fabricated in which a SAM is formed in a pore patterned in a dielectric, with a conductive polymer spin-deposited onto the monolayer prior to the deposition of a metal contact. This technique achieves high device yield and has been used to measure monolayers of alkanethiols, alkanedithiols, and paraphenyls;[9,19,22,23] however, it has so far only been demonstrated in the fabrication of devices 1 μm or larger. The present work demonstrates such a molecular electronic device structure with submicrometer dimensions, high yield, and compatibility with any molecular structure that can be assembled on a surface.

RESULTS AND DISCUSSION

Fabrication and SAM Formation. The key development of the present work is the submicrometer scaling of polymer-contacted devices. This is achieved by confining the SAMs to pores in an inorganic, rather than photoresist, dielectric, then applying a low-viscosity, amphiphilic conductive polymer onto the monolayer prior to deposition of a metallic top contact. A schematic of a representative device and scanning electron microscope (SEM) and atomic force microscope (AFM) characterizations are presented in Figure 1.

We modify the fabrication process described by Akkerman *et al.*, by replacing the photoresist layer with an inorganic dielectric deposited through conformal coating methods. There are several drawbacks to a photoresist dielectric. First, organic dielectrics prevent the use of standard procedures such as oxygen plasma or peroxysulfuric acid etching ("piranha" etch) to remove adventitiously adsorbed carbon on the gold surface prior to monolayer formation. Second, the resist layer may swell or even partially dissolve in some of the common solvents used to deposit monolayers. It has been shown that photoresist dielectric layers can be baked to render them resistant to both ethanol and tetrahydrofuran;[19] however, high-temperature treatment may result in distortion of small features patterned in the resist layer. Finally, the photoresist layer must be deposited in an extremely clean environment, with sufficient thickness to avoid pinhole leaks and shorting from dust particles. In the present work, it was found that a resist dielectric must be at least several hundred nanometers thick to avoid leaks. Nanoscale pores in such a dielectric have high aspect ratios and suffer from poor wetting by monolayer formation solutions and conductive polymers. In contrast, a conformal inorganic dielectric deposition method such as ALD or plasma-enhanced chemical vapor deposition (PECVD) can achieve a pristine dielectric layer a few nanometers thick even when deposited outside a cleanroom environment, yielding pore structures that can be wetted more easily.

Following previous work which used larger pores, we initially attempted to use aqueous PEDOT:PSS as a conductive interface between the SAM and evaporated metal contact.[9] However, we find that the polymer will not fill pores with diameters smaller than a few micrometers, even with the addition of surfactants. Better results are found with Aedotron P, a commercially available conductive polymer dispersed in an organic solvent. The particular Aedotron blend used in the present work is a block copolymer of PEDOT and polyethylene glycol dissolved in nitromethane and doped with *p*-toluene sulfonate.[28] We find that the low viscosity and superior wetting of nitromethane allows the deposition of the polymer into pores as small as 100 nm in diameter and 50 nm deep. A few other blends of Aedotron are also investigated but prove ineffective for the present work. Aedotron C, a mixture that uses propylene carbonate solvent, fails to penetrate submicrometer pores. Aedotron C3, a highly conductive blend of polymer in nitromethane, results in shorted devices.

A key trade-off in the use of Aedotron P in place of PEDOT:PSS is the higher resistivity of the new polymer. At room temperature, the specific contact resistance of polymer-only devices (SAM omitted) is 6 m$\Omega\cdot$cm^2, or 800 kΩ for a 1 μm diameter pore, a resistance on the order of the least resistive molecular junctions investigated in this study. To illustrate the resulting low current density of the Aedotron P devices in this work,

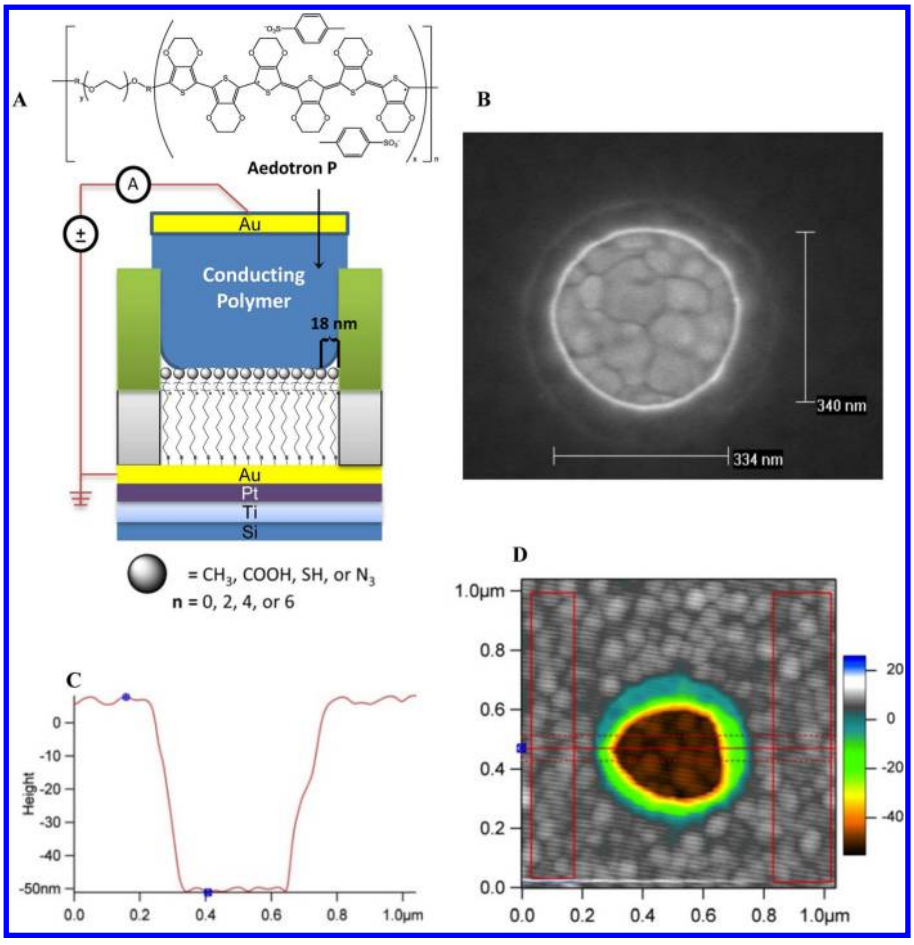

Figure 1. (A) Device schematic (not to scale). (B) SEM image of 340 nm diameter pore before monolayer formation or polymer deposition. (C) Cross section, illustrating dielectric thickness of 60 nm. (D) AFM scan of pore before monolayer formation or polymer deposition.

TABLE 1. Current Density at 1 V Bias for Octanedithiol SAM Devices with Metallic, PEDOT:PSS, and Aedotron P Top Contacts[26] and Control Devices with No Monolayer and Only PEDOT:PSS or Aedotron P Layers[27]

device	metal SAM	PEDOT:PSS SAM	Aedotron SAM	PEDOT:PSS only	Aedotron only
J at 1 V (A/cm^2)	400000	300	50	5000	200

Table 1 presents a comparison of the measured current density of Aedotron P and PEDOT:PSS devices with and without octanedithiol ($HS(CH_2)_8SH$) SAMs,[26,27] as well as devices with metallic top and bottom contacts, with 1 V applied bias. The Aedotron devices were fabricated in this work, while the data for PEDOT:PSS and metallic devices were reported by other groups in prior papers. We see that devices containing only Aedotron P exhibit lower current density than either metallic or PEDOT:PSS-contacted devices containing SAMs.

At room temperature, the polymer exhibits ohmic behavior and the molecular device transport behavior resembles that seen in other molecular tunnel barriers. As will be discussed in a later section, at lower temperatures, the molecular device behavior is dominated by the accessibility of sites for carriers at the interface of the polymer layer and monolayer. The fabrication parameters are detailed in the Methods section, and the full process is illustrated in Figures S7 and S8 in the Supporting Information.

Transport Measurements. The devices are first studied by measuring the current density, J, through a series of alkanethiol SAMs of varying length (Figure 2). The gold substrate is grounded, with electrical potential bias V, applied to the polymer contact. Each data point in Figure 2 represents the geometric mean of at least 13 devices. Monolayers are formed in pores of either 1 μm or 300 nm diameter. The measurements are performed at room temperature under vacuum. Before calculating the geometric mean, shorted and outlying devices are discarded from the data set. Under optimized fabrication conditions, as discussed in the Methods section, the yield of devices per chip ranges from 70 to 100%. Outlying devices from each set are then removed by eliminating the most and least conductive 1/6 of the remaining devices.

The apparent current density for a given monolayer thickness systematically varies between the 1 μm and 300 nm diameter pores, with the smaller pores having

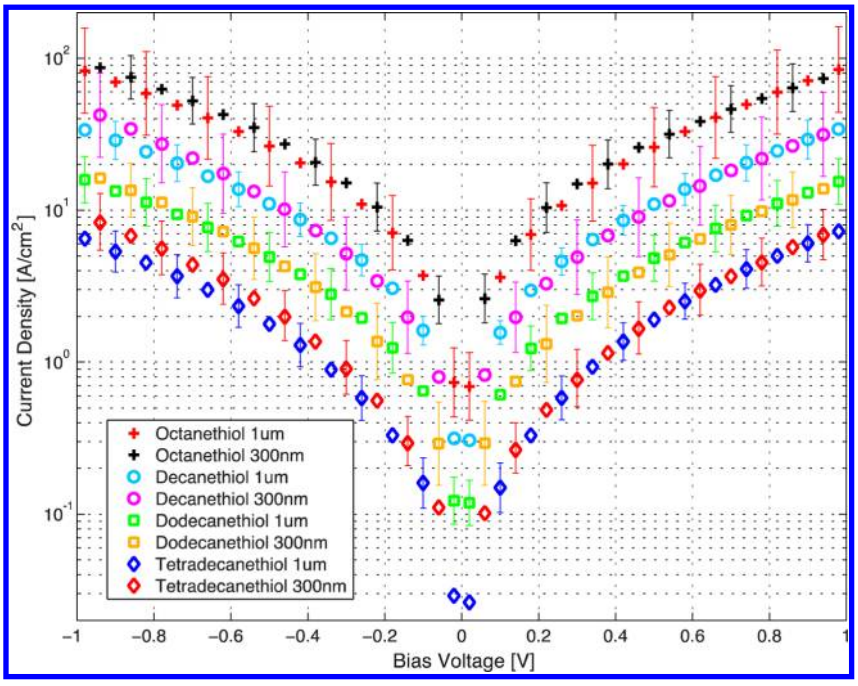

Figure 2. Current densities of 1 μm and 300 nm diameter pores containing SAMs of $CH_3(CH_2)_7SH$, $CH_3(CH_2)_9SH$, $CH_3(CH_2)_{11}SH$, and $CH_3(CH_2)_{13}SH$, measured at room temperature under vacuum.

slightly lower current densities. We theorize that the 300 nm diameter pores are effectively smaller than their measured dimensions. The exposed gold on the bottom of the pores may not span the entire patterned area; meniscus formation may prevent the polymer from fully filling the pore, or the polymer "plug" may shrink during vacuum drying after deposition. For the purposes of modeling, we surmise the existence of an 18 nm rim of uncontacted area, effectively reducing the device diameters to 0.96 μm and 264 nm, as illustrated in the device schematic (Figure 1A). The inferred current densities in both pore sizes correspond roughly to those reported for larger devices with PEDOT:PSS top contacts.[9] Hence, in the remainder of the paper, this "uncontacted rim" correction is always applied, though it does not affect any of our key conclusions. In both control devices with only Aedotron P and devices containing SAMs, we find that the conductance at first varies significantly as a function of duration under vacuum, likely due to the evaporation of solvent from the Aedotron P. The effect saturates after 2 h, and devices measured from several hours up to several days under vacuum demonstrate consistent behavior. Thus, each device is maintained under vacuum for 4 h prior to measurement. SAM-containing devices that are not dried under vacuum demonstrate substantially asymmetric current density *versus* bias curves, with higher current density observed under reverse bias. They also often demonstrate substantial hysteresis.

The conductance of working devices on a given chip varies with a log-normal distribution. The measured current density at 1 V bias of every device analyzed in Figure 2 is presented as a scatter plot in Figure 3. The median current density for a given set of devices (horizontal red line in each box) is typically close to the geometric mean (enlarged data point in each set). Given that the conductance of a tunnel barrier varies as an exponential function of barrier thickness, we hypothesize that the log-normal distribution is due to a normal distribution in the effective barrier thickness from one pore to the next.

Numerous experimental and theoretical studies have found that nonresonant, through-bond tunneling is the transport mechanism through an alkanethiol SAM in a molecular junction. Thus, we anticipate that the current density, *J*, will be exponentially dependent on the SAM thickness, which can be represented by the number of carbons in the molecular species.[29] Figure 4 presents the current density as a function of the number of carbons in the alkanethiol species at 0.1, 0.3, and 0.5 V biases. Fit lines are described by the following equation:

$$J = A^{*}\exp(-\beta_c n) \quad (1)$$

where *J* is the current density, *A* is an arbitrary constant, β_c is the decay parameter, and *n* is the number of carbons in the alkane chain. We note a slight decrease of β_c with increasing bias, in accordance with theoretical calculations of transport through a tunnel barrier.[8]

We find β_c values of 0.55, 0.51, and 0.45 per carbon at a bias of 0.1, 0.3, and 0.5 V, respectively. These values are substantially lower than most reported values in the literature. Experimental and theoretical values of β_c for alkane transport at low bias are typically ~1, in both solid-state[30−32] and electrochemical measurements.[33]

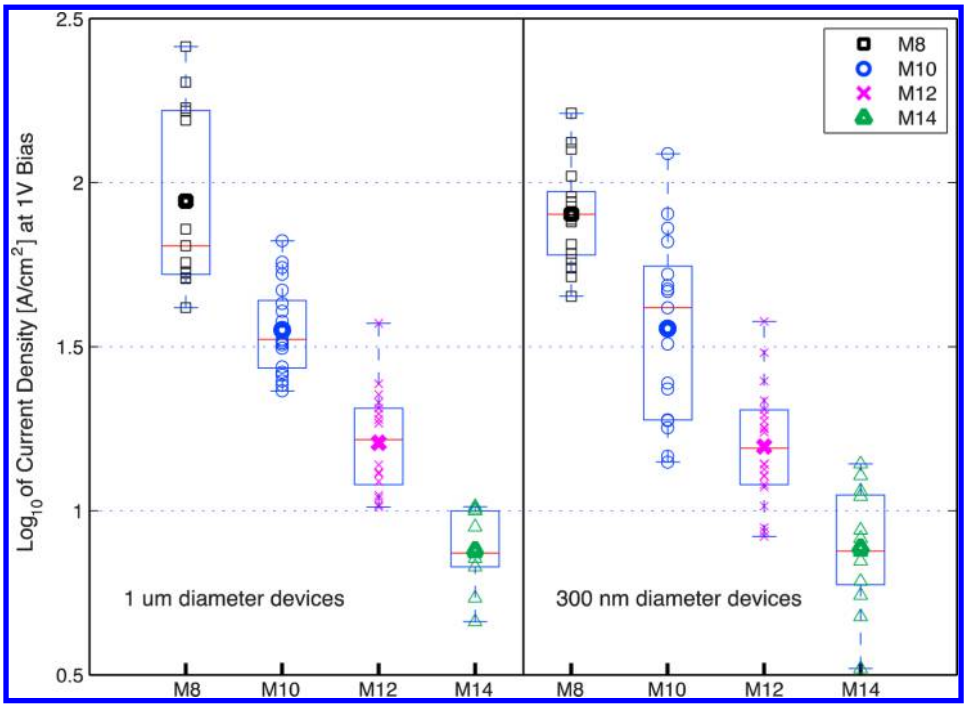

Figure 3. Scatter plot overlaid on box and whiskers plots of the common logarithm of the measured current density for 8, 10, 12, and 14 carbon alkanethiols in 1 μm diameter (left) and 300 nm (right) devices, as presented in Figure 2 (but corrected for uncontacted area). The red horizontal line in each box is the median for the set, the top and bottom of each box correspond to first and third quartiles, and the dashed lines stretch to the furthest outliers. Measurements are taken at room temperature under vacuum. The plot demonstrates the log-normal distribution for each set of devices and the exponential decay of current density as a function of increasing molecule length.

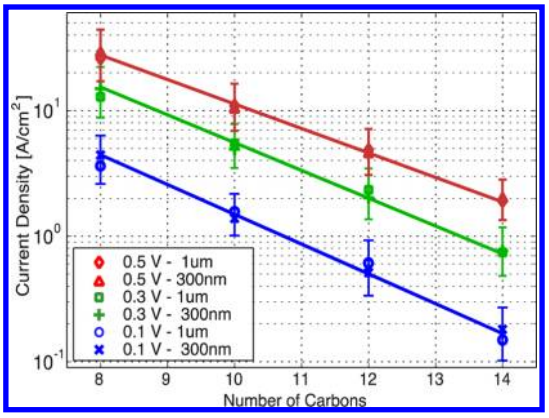

Figure 4. Current density and exponential fit of data as a function of number of carbons in the alkanethiol tail at 0.1, 0.3, and 0.5 V bias. Fit lines are of the form in eq 1.

We are aware of only three prior experimental reports of $\beta_c < 0.8$ for alkanes out of dozens of studies in the literature. One of those reports, based on AFM probing of gold nanoparticles deposited on alkanedithiol SAMs, initially found $\beta_c = 0.58$.[34] However, the authors later attributed their findings to Coloumb blockade effects and revised the value to $\beta_c = 0.95$ in a subsequent study.[35] Another low value ($\beta_c = 0.52$) was reported for measurements of single dithiols using an STM tip above a gold surface in solution.[36] The reason for this anomalous result is unclear, but it is in disagreement with several similar studies of both dithiol and diamine alkanes in STM break junctions.[30] Most relevant to the current study, Akkerman *et al.* found $\beta_c = 0.66$ at 0.1 V for alkanedithiols with PEDOT:PSS top contacts in a device geometry similar to that of the present work.[9] The same research team later reported $\beta_c = 0.9$ for alkanethiol monolayers but noted that the relationship only held for alkanethiols with more than 14 carbons, with β_c effectively equal to 0 below this length.[37] We theorize that in both the present work and Akkerman's studies of alkanethiols, the polymer contact may be penetrating into the monolayer at defect sites. Whitesides *et al.* have previously shown that the presence of even a small percentage of "thin-area" defects, typically present at grain boundaries and raised vacancy islands, can substantially affect the current measured through a monolayer junction.[38] We note that such penetration does not happen in all experiments that use soft contacts, as Milani *et al.* found $\beta_c = 1.13$ for devices with undoped polyphenylenevinylene spin-coated from a dispersion in chloroform onto 8−16 carbon alkanethiols on gold.[22] Monolayer defect penetration appears to occur when strongly wetting polymers are applied to SAMs shorter than 16 carbons.

One benefit of the superior wetting of Aedotron P is the material's compatibility with any SAM termination. Figure 5 presents the current density measured at 1 V bias for devices containing 8- and 12-carbon alkanethiols terminated with methyl (M8, M12), thiol (T8, T12), and carboxyl (C8, C12) groups, as well as $N_3(CH_2)_{11}SH$ (A11). The methyl-, carboxyl-, and azide-terminated molecules

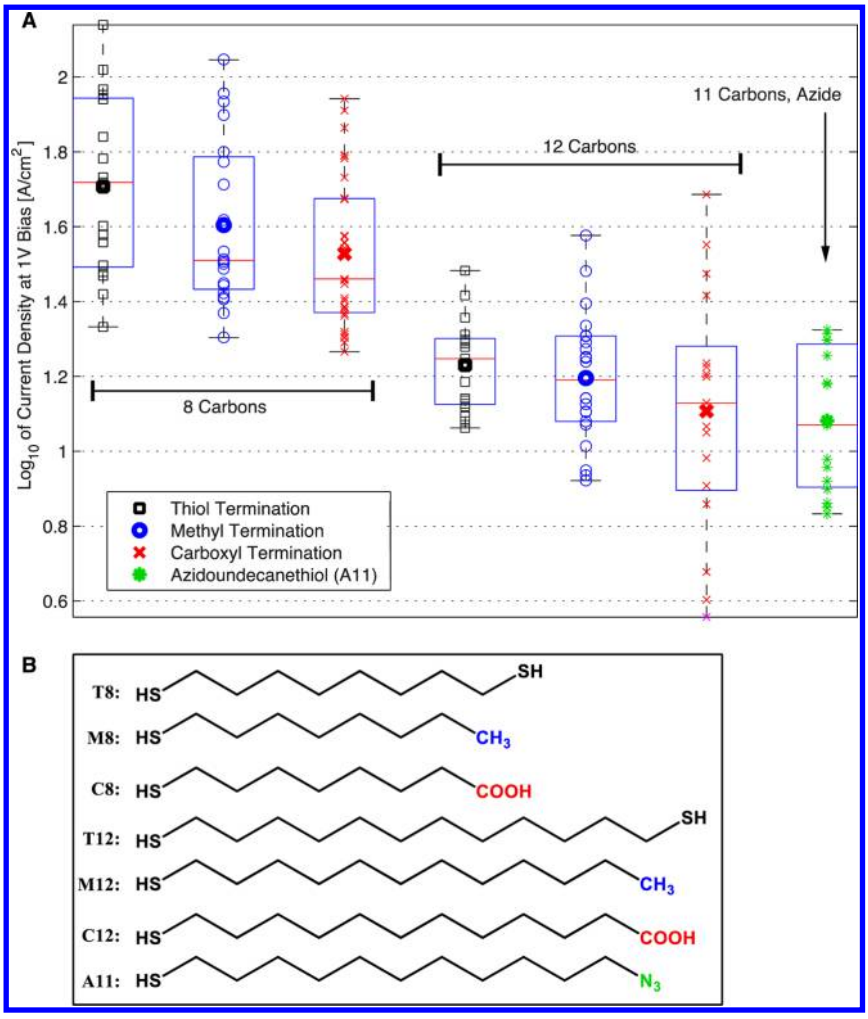

Figure 5. (A) Box and whiskers plots showing medians, quartiles, and outliers overlaid on scatter plots of current density at 1 V bias for $HS(CH_2)_8SH$ (T8), $CH_3(CH_2)_7SH$ (M8), $HOOC(CH_2)_7SH$ (C8), $HS(CH_2)_{12}SH$ (T12), $CH_3(CH_2)_{11}SH$ (M12), $HOOC(CH_2)_{11}SH$ (C12), and $N_3(CH_2)_{11}SH$. Measurements are taken at room temperature under vacuum. The large data point for each scatter plot set indicates the geometric mean. (B) Measured alkane species.

all display similar current density for a given monolayer thickness, while the dithiols, particularly $HS(CH_2)_8SH$, are somewhat more conductive. This may be due to the propensity for alkanedithiol molecules to fold over with both terminal thiols bound to the gold surface, resulting in an effectively shorter monolayer. While previous work has shown that SAM formation with concentrations of greater than 30 mM minimizes this tendency,[23] it is not clear that it can ever be completely avoided.

Temperature Dependence. To better understand the role of the polymer top contact in transport, and to establish another comparison between Aedotron P and PEDOT:PSS-contacted devices, a subset of devices is characterized across a range of temperatures. According to the Simmons model description of transport between two metallic contacts through a tunnel barrier in a low bias regime,[39−41] the current density through a SAM at a fixed bias should only vary by a few percent as the device is cooled from room temperature to 0 K. This behavior has been observed in numerous experimental studies.[10,14,40,42] In contrast, in the present study we find that the current density varies by orders of magnitude as the device is cooled below room temperature, in agreement with previous measurements of junctions with polymer top contacts.[19] Accounting for the polymer contact as a simple series resistance fails to explain the observed behavior. Instead, we find that an Arrhenius plot of the SAM current looks qualitatively similar to that of the polymer control devices, indicating that a similar mechanism controls transport in both systems.

Figure 6A presents the current density as a function of voltage at various temperatures in a representative 30 μm diameter device containing only a polymer layer and no SAM. As the device is cooled, its conductance decreases and transport becomes non-ohmic. Figure S9 in the Supporting Information presents similar data over a range of −1 to 1 V. Figure 6B presents an Arrhenius plot of selected data points from Figure 6A.

Examining the data in Figure 6B, for each curve we see two regimes of temperature dependence, suggesting a unique mechanism for transport in each regime. The high-temperature behavior is a traditional Arrhenius

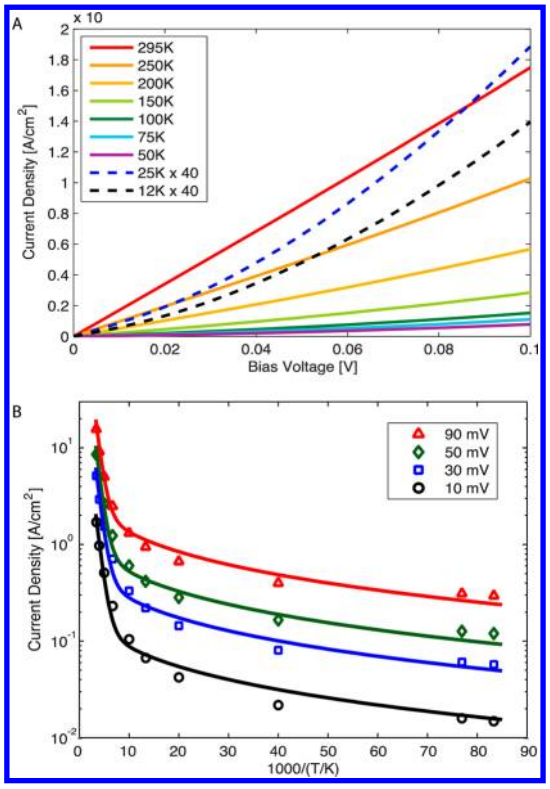

Figure 6. (A) Current density as a function of bias for 30 μm diameter polymer-only device at various temperatures. For visibility, 25 and 12 K traces have been multiplied by a factor of 40. Below 200 K, Aedotron P demonstrates increasingly non-ohmic transport behavior. (B) Arrhenius plot of selected data points from A, with overlaid fit lines described by eq 2.

curve, with the current declining as an exponential function of the inverse temperature. This section can be described with amplitude σ_{ARR} and slope ΔE. The subscript ARR is chosen because the observed behavior is Arrhenius-like. We find that the current at low temperature can be described as an exponential function of $T^{-1/4}$, as in a variable-range hopping process, with amplitude σ_{VRH} and characteristic energy, E_0. The subscript VRH is chosen because the behavior is similar to variable-range-hopping. As we vary the applied bias, the strength of both processes varies relative to one another, so we choose a purely empirical form crossing from linear to exponential conductance at a different characteristic voltage scale for each of the two processes. This yields fit lines that are collectively described by the following equation, with parameter values held fixed across all four curves in Figure 6B:

$$J(T,V) = \sigma_{ARR} V \cosh(V/V_{ARR}) \exp(-\Delta E/kT) + \sigma_{VRH} V \cosh(V/V_{VRH}) \exp(-(E_0/kT)^{1/4}) \quad (2)$$

where the two addends describe the high- and low-temperature transport regimes; k is the Boltzmann constant, T is the temperature, and V_{ARR} and V_{VRH} are measures of the nonlinearity of each channel, assumed to be symmetric with respect to the applied bias.

TABLE 2. Values of Fit Parameters Used in Figures 6BB and 7 To Model the Current Density as a Function of Both Voltage and Temperature for Polymer-Only, $CH_3(CH_2)_7SH$, and $CH_3(CH_2)_{11}SH$ SAM Devices, Respectively, Using Equation 2

device	σ_{ARR} (S/cm^2)	σ_{VRH} (S/cm^2)	ΔE (meV)	E_0 (meV)	V_{ARR} (V)	V_{VRH} (V)
polymer	6120	98.4	90	305	>100	0.079
$CH_3(CH_2)_7SH$	1083	0.20	97	310	0.50	0.21
$CH_3(CH_2)_{11}SH$	308	0.27	92.3	309	0.52	0.221

The described voltage dependence is similar to that found in studies of other organic conductors.[43−47] σ_{ARR} and σ_{VRH} describe the conductance of each channel in the limit of high temperature. ΔE and E_0 describe the characteristic energy of each channel. At this time, we have no physical interpretation for V_{ARR} or V_{VRH}. The values of the fit coefficients are presented in Table 2.

We anticipate carrier thermalization in the bulk of the polymer layer, so it is appropriate to treat the SAM−polymer structure of a full device as a nonlinear voltage divider. We assume that the same current *versus* bias function applies to the bulk of the polymer when it is on the SAM as when it is on just gold. For temperature-dependent measurements of SAM-containing devices, for each measured current density, we empirically determine the voltage drop across the polymer layer, V_{poly}, and subtract this value from the applied bias, V_{app}, to determine the voltage across the monolayer, $V_{SAM} = V_{app} - V_{poly}$. As the polymer resistance is ohmic, but the SAM has an exponential JV relationship, at low voltages, the SAM layer accounts for a greater percentage of the voltage drop in the device. Thus, for $CH_3(CH_2)_7SH$ devices at room temperature, the percentage of applied voltage dropped across the polymer (*i.e.*, V_{poly}/V_{app}) ranges from 10 to 30% as the applied bias ranges from 0 to 1 V. For $CH_3(CH_2)_{11}SH$ devices, V_{poly} ranges from 4 to 10% as the applied bias increases from 0 to 1 V.

Figure 7A plots the average measured current density as a function of inverse temperature for a single 300 nm diameter device containing a $CH_3(CH_2)_7SH$ SAM with V_{SAM} of 0.1, 0.3, 0.5, and 0.9 V (corresponding to V_{poly} of 0.017, 0.08, 0.16, and 0.36 V, respectively).[48] Figure 7B presents data from the mean of an identical measurement on a set of three devices containing $CH_3(CH_2)_{11}SH$ SAMs. At low temperature and low bias, the signal cannot be isolated from the background noise and those data points are not included in either plot. Data at each value of V_{SAM} is fit by a series of curves using eq 2. The values of the fit coefficients are presented in Table 2.

When the data in Table 2 are examined, σ_{ARR} is the only parameter that systematically varies between the two molecule lengths, indicating that the other parameters are determined by the polymer transport behavior. Although the extracted σ_{ARR} value is sensitive

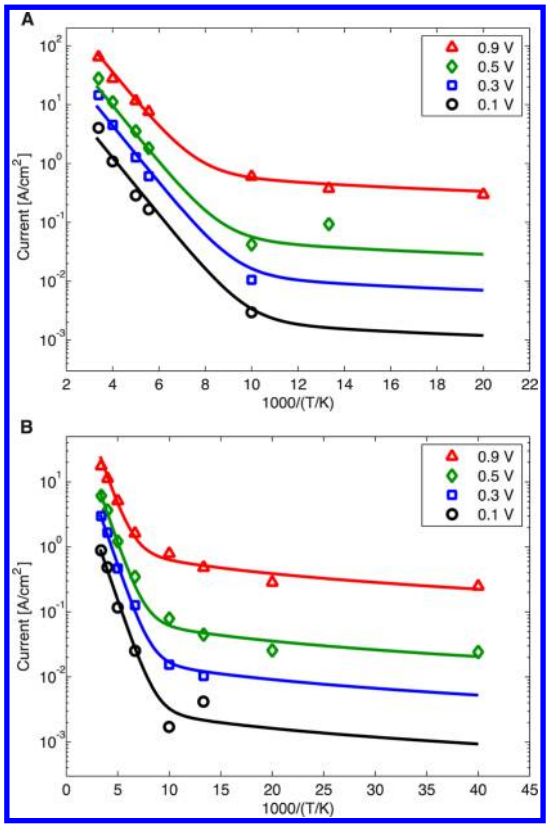

Figure 7. (A) Arrhenius plot of representative 300 nm diameter $CH_3(CH_2)_7SH$ device conductivity as a function of temperature at various calculated monolayer voltages, V_{SAM}. Overlaid solid lines are fits in the form of eq 2. The reported bias is empirically determined voltage across the monolayer, calculated by subtracting the polymer voltage drop from the applied bias at each measured point. (B) Identical measurement to that presented in (A) but performed on a set of three devices containing $CH_3(CH_2)_{11}SH$ SAMs. Each data point represents the mean of the three devices.

to small changes in the value of ΔE used in the fit, we can observe that it is roughly proportional to the measured room temperature current, indicating that it is exponentially related to the SAM thickness, as observed in Figure 4 and eq 1. The energy scales ΔE and E_0 are consistent between polymer-only and SAM devices. The presence of a SAM is reflected in the significant drop in the device conductance coefficients, particularly in σ_{VRH}, and in the shift from a low resistance ohmic bias dependence at high temperature (large V_{ARR}) to a higher-resistance linear-exponential behavior (small, similar magnitude V_{ARR} and V_{VRH}), as observed at room temperature in Figure 2.

The observed polymer-only and SAM temperature dependence is consistent with the low-temperature behavior of both SAM and polymer-only devices being governed primarily by the accessibility of states in the polymer as a function of energy. In a disordered material such as a conductive polymer like PEDOT:PSS or Aedotron P,[43] localized trap states exist from the bottom of the conduction band up to a critical energy E_c, called the mobility edge.[49] Charge transport between localized trap states occurs *via* thermally activated hopping, a process known as variable-range hopping because the typical hops become longer with decreasing temperature and electric field. For a three-dimensional material, variable-range hopping gives a conductivity varying as an exponential function of $T^{-1/4}$, consistent with the low-temperature behavior observed in the present devices. Above the mobility edge, states become nonlocalized or extended, and transport is equivalent to carrier drift seen in single-crystal semiconductors, with carriers freely accelerating under the applied field before reaching a constant average velocity due to scattering from impurities and phonons. At high temperatures, we expect extended state transport to dominate over hopping in the polymer. Current is carried by electrons excited to the mobility edge, with the Boltzmann distribution of the carriers yielding the high-temperature Arrhenius behavior observed in all of the devices.[49]

While the above description of temperature- and bias-dependent transport is physically intuitive and captures the key features of our data, the observed behavior can also be described with a model of dissipative quantum tunneling through a potential barrier, as previously shown by Kronemeijer *et al.*[19,50] In this conceptualization, the transport is characterized by a power-law dependence on both bias and temperature. This model was previously employed to describe transport in one-dimensional Luttinger liquids such as carbon nanotubes.[51] While the model was originally thought to apply to polymer systems only if they consisted of long one-dimensional chains, such as PBTTT,[52] further studies have shown that the model also empirically describes transport in polymers consisting of distinct microscopic grains such as PEDOT:PSS,[50] as well as molecular junctions of the kind described in the present work.[19] It is not clear why a model of a one-dimensional system describes transport through a disordered three-dimensional series of grains in a conductive polymer, nor can we ascertain the mechanism of the dissipation assumed in the model. Furthermore, it is uncertain whether the potential barrier being described is the SAM or that between localized sites in the polymer. With these caveats in mind, this model does produce curves that accurately and economically fit the data, and we find report extracted fit parameters in order to compare with those published for PEDOT:PSS-contacted devices.

The dissipative tunneling model defines the tunneling current density J as:[53,54]

$$J = J_0 T^{1+\alpha} \sinh(\gamma(eV/kT)) |\Gamma(1 + \alpha/2 + i\gamma(eV/\pi kT))| \quad (3)$$

where α, J_0, and γ are fit parameters, V is the applied bias, e is the elementary charge, k is the Boltzmann constant, and Γ is the Gamma function; α can be

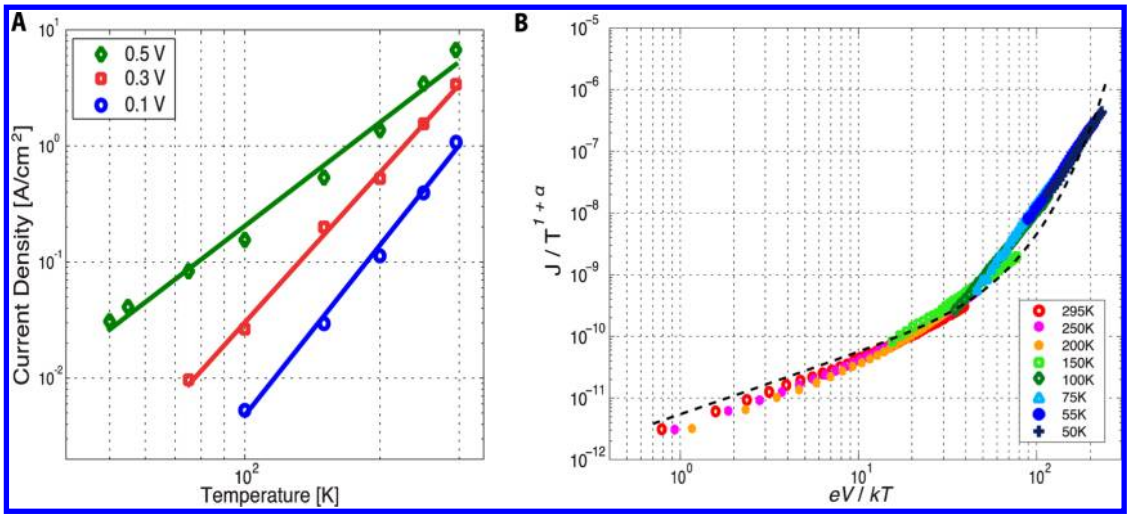

Figure 8. (A) Current density as a function of temperature for a given bias plotted on a double logarithmic scale. (B) Scaled current density presented on a double logarithmic scale as a function of *eV/kT*. The solid curve is calculated with eq 3 using $\alpha = 5.0$, $\gamma = 0.048$, and $J_0 = 4 \times 10^{-15}$A/cm^2.

considered as a relative measure of the effect of temperature on transport. The temperature is normalized per Kelvin. It has been demonstrated that J_0 varies substantially as a function of the length and barrier height of the SAM. In the case of Luttinger liquid transport, γ describes the distribution of potential across the tunnel barriers between the contacts and the one-dimensional transport channel;[51] however, the appropriate physical interpretation is not clear for a molecular junction with a polymer contact. Temperature-dependent measurements of larger molecular junctions containing a variety of paraphenylthiol and alkanethiol molecules under PEDOT:PSS top contacts yielded values of $\alpha = 2$ to 3, $J_0 = 2 \times 10^{-10}$ to 1×10^{-4} A/cm^2, and $\gamma = 0.02$ to 0.03.[19]

Figure 8A plots the current density of a representative $CH_3(CH_2)_{11}SH$ SAM device at 0.1, 0.3, and 0.5 V bias *versus* temperature on a log−log scale. Data at each bias can be fit to a straight line, indicating that the observed temperature dependence also fits a power law. The slope increases as a function of decreasing bias. By extrapolating the fit lines to a bias of 0 V, eq 3 reduces to $J = J_0T^{1+\alpha}$, yielding $\alpha = 5.0$. In Figure 8B, we use this derived value of α to scale the current density across all measured temperatures, and we observe that the data measured across a range of temperatures collapse onto a single curve. The *y*-axis, defined by $J/T^{1+\alpha}$, spans 6 orders of magnitude. The *x*-axis, defined with the dimensionless parameter *eV/kT*, spans 2.5 orders of magnitude. Fitting a line described by eq 3 to the data, we extract the parameters $\gamma = 0.048$ and $J_0 = 4 \times 10^{-15}$A/cm^2. Data points corresponding to current density less than 0.01 A/cm^2 have been removed because they fall below the noise limit of our measurement electronics. While the emergence of a universal curve and the precision of the determined fit are not as unambiguous as previous results, we feel reporting the fits is useful in comparing this device's extracted parameters with those previously reported for larger-area junctions.

The value we obtain for α is substantially higher than that reported for PEDOT:PSS devices,[19] indicating that transport in Aedotron P devices is substantially more dependent on temperature. This may be due to the fact that Aedotron P is more resistive than PEDOT:PSS, and thus variation in the polymer resistance is more noticeable in our devices. We next observe that J_0 in the present device is several orders of magnitude lower than values reported for PEDOT:PSS. As J_0 simply positions the fit curve vertically along the $J/T^{1+\alpha}$ axis, the substantial change is explained by the exponential dependence of J_0 on α. Finally, we note that the extracted value of γ in this series is roughly double that reported for paraphenylthiol and alkanethiol devices with PEDOT:PSS contacts. As noted in prior work,[19,50] it is not clear how to physically interpret this parameter.

CONCLUSIONS

We have demonstrated a two-terminal nanoscale molecular electronic structure with high yield and the previously unavailable flexibility to incorporate any self-assembled monolayer. We have explored the conductivity of alkanethiols with a variety of terminations and examined the temperature dependence of transport in our devices, finding that the polymer contact plays a dominant role at low temperatures. We have presented a transmission model of transport in the device and shown its applicability to varying molecular lengths and temperatures. The reported results demonstrate that the present device structure resolves various limitations of previous molecular junctions incorporating conductive polymer contacts, while maintaining their high yield and extending their

compatibility with a variety of molecular systems. A drawback of this device structure is the high contact resistance of Aedotron P, which could dominate the current−voltage behavior in some circumstances, for instance with SAMs that are significantly more conductive than the alkanethiols studied in this work.[55]

Future investigations may explore the conductivity of conjugated and mixed monolayer systems, studying the role of molecular structure and monolayer packing on transport, and examine rectifying and switching behavior in specially tailored molecules. Finally, aggressively scaling the present structures to the limits of lithographic patterning may enable the realization of high-yield, low-variation molecular devices at size scales beyond the physical limitations of semiconductor materials.

METHODS

Pore Fabrication. The device fabrication begins with the deposition of 7, 30, and 150 nm of titanium, platinum, and gold, respectively, onto a highly doped silicon wafer with a resistance of 5 mΩ·cm with 1000 Å thermal oxide. Each layer is evaporated a rate of 1 Å/s in an e-beam evaporator evacuated to 3×10^{-7} Torr. The platinum layer is essential in preventing diffusion of the titanium and gold layers during the 350 °C nitride deposition process, which otherwise results in dielectric pitting and shorting. The gold layer root mean square roughness is 1.2 nm (Figure S6 in Supporting Information) measured with an Asylum Research Molecular Force Probe 3D AFM. Next, 20 nm of alumina (200 cycles) is deposited by ALD in a Cambridge Nanotech system followed by 40 nm of silicon nitride deposited by PECVD for 4.5 min in an STS PECVD system.

A layer of ZEP-520A or bilayer of PMMA/MMA e-beam resist is then spun onto the wafer. The resist is applied with a 5 mL syringe with a 0.2 μm particle filter. The spin speed is chosen such that the resist thickness is roughly equivalent to the desired diameter of the pores. For the fabrication of 300 nm devices, undiluted ZEP-520A is spun at 5000 rpm. For the fabrication of 1 μm devices, a bilayer of Microchem EL 11 MMA copolymer under PMMA 950 A5 is spun at 3000 rpm for each layer. After each layer of resist is applied, the sample is baked at 180 °C (PMMA/MMA) or 200 °C (ZEP) on a hot plate in ambient for 2 min. The resist is exposed in a Philips XL30 SFEG field-emission scanning electron microscope controlled by a Nabity Nanometer Pattern Generation System, at a dose of 400 μC/cm^2. Wafers containing dozens of devices with exposed resist are stored under nitrogen. Over several months of experiments, chips are cleaved from the wafer as needed, and the proceeding steps are performed on batches of a few to a dozen chips.

The resist is developed for 40 s in 3:1 isopropyl alcohol/methyl isobutyl ketone (PMMA/MMA) or for 1 min in ZED-N50 developer (ZEP), and then cured for 10 min on a hot plate at 110 °C. To ensure the integrity of the etch mask, a low-angle metal mask evaporation technique has been adapted from previous work.[56] Chrome (2 nm) and nickel (5 nm) are evaporated at an angle of 14° from the plane of the surface while rotating the sample such that the resist surface is covered with a thin layer of metal while preventing the penetration of metal into the patterned pores.

The nitride layer is then etched for 70 s in an MRC reactive ion etcher at a rate of ∼0.8 nm/s using 18 sccm of CHF_3 and 2 sccm of O_2 at 10 mTorr with 100 W power. It is found that this etch not only exposes but also compacts the alumina layer, reducing it to a thickness of a few nanometers. However, the etch never penetrates the alumina, even after several minutes of etching. The residual few nanometers of alumina is removed with a 10 s wet etch in 20:1 dilute buffered oxide etch (BOE), revealing gold that is uncontaminated by any ion residue, as confirmed by XPS (Figures S1−S4). In devices in which the alumina buffer layer is not used and nitride on gold is simply dry etched, the gold is invariably contaminated by implanted silicon from the nitride layer, which results in poor monolayer formation.

The formation of densely packed monolayers is verified by electrochemical oxidation of ferrocyanide using an array of 1 μm pores as the working electrode.[24,25] The formation of a dense SAM slows the electron transfer to the gold surface at the bottom of the pores, evidenced by a significant reduction in the oxidative current (Figure S5 in the Supporting Information).

Monolayer Formation. Prior to monolayer formation, the chips are exposed to O_2 plasma for 5 min to oxidize the top atomic layer of exposed gold atoms at the bottom of each pore and remove any adventitiously adsorbed carbon.[57] The chips are then immersed in 200 proof ethanol (Acros) for 20 min to reduce the oxidized gold layer. They are then transferred to a 50 mM solution of the appropriate molecule in ethanol and left for 48 h under inert atmosphere. The devices are then removed and rinsed in 200 proof ethanol and CMOS grade isopropyl alcohol.

Contact Deposition. Immediately after rinsing, the devices are reintroduced into a nitrogen-filled glovebox. Aedotron P (1% poly(3,4-ethylenedioxythiophene)-*block*-poly(ethylene glycol)) solution in nitromethane with sulfonate *p*-toluene as a dopant is deposited onto each chip and then spun at 1000 rpm for 15 s before acceleration to 2000 rpm for another 30 s. This results in a 90 nm thick polymer layer. The devices are then dried under vacuum for 4 h. Top gold contacts (100 nm) are evaporated onto the devices through shadow masks, and the residual polymer is removed using oxygen plasma for 1 min.

Measurement. The devices are measured under vacuum using a Desert Cryogenics (now Lake Shore) flow cryostat probe station and a Keithley 2400 source meter; 34−47 devices are fabricated per chip, with a yield ranging from 70 to 100%. Failed devices are typically shorts or exhibit orders of magnitude higher conductivity than a typical device. The failures are due to defects in the resist layer, which are then transferred to the mask, resulting in shorts or excessive device area. This is evidenced by the improvement yield when the resist is filtered before application.

The conductance of Aedotron P varies significantly as a function of duration under vacuum, although the effect saturates after a few hours. Thus, each device is maintained under vacuum for 4 h prior to measurement. Devices that are not dried under vacuum demonstrate substantially asymmetric current density *versus* voltage curves, with higher current density observed under reverse bias. These devices often show substantial hysteresis.

For measurements at varying temperature, the devices are placed under vacuum for 4 h and then cooled to 25 K over 30 min as liquid helium is pumped through the cryostat. Using a heating element inside the cryostat stage, the devices are then warmed back up to room temperature over a period of a few hours, with measurements taken at each temperature reported in the text.

Conflict of Interest: The authors declare no competing financial interest.

Acknowledgment. The authors are pleased to thank S. Wind, H. Akkerman, A. Kronemeijer, and M.A. Kastner for helpful discussions, T. Carver for technical advice, and J. Bloking for technical advice and providing the results of Aedotron P photospectroscopy measurements. This work was supported through the Center on Nanostructuring for Efficient Energy Conversion (CNEEC) at Stanford University, an Energy Frontier Research Center funded by the U.S. Department of Energy, Office of Science, Office of Basic Energy Sciences under Award Number DE- SC0001060. Fabrication work was performed in part at the Stanford Nanofabrication Facility (a member of the

National Nanotechnology Infrastructure Network) supported by the NSF under Grant ECS-9731293. Fabrication work was also performed at the E.L. Ginzton Laboratories Flexible Cleanroom, located in the Stanford Nano Center.

Supporting Information Available: XPS data for the composition of freshly evaporated gold surface, PECVD SiN, gold after SiN reactive ion etch and gold after two-step etch process. Cyclic voltammetry plots demonstrating monolayer packing in an array of pores. AFM scan demonstrating gold roughness. Pore fabrication process, monolayer formation, and top-contact deposition. Full range *JV* plots as a function of temperature for polymer-only devices. This material is available free of charge *via* the Internet at http://pubs.acs.org.

REFERENCES AND NOTES

1. Thompson, S.; Parthasarathy, S. Moore's Law: The Future of Si Microelectronics. *Mater. Today* **2006**, *9*, 20–25.
2. Tour, J. M. Molecular Electronics. Synthesis and Testing of Components. *Acc. Chem. Res.* **2000**, *33*, 791–804.
3. Lundstrom, M. Applied Physics. Moore's Law Forever? *Science* **2003**, *299*, 210–211.
4. Ellenbogen, J. C. Monomolecular Electronic Device. U.S. Patent 6,339,227, 2002.
5. Joachim, C.; Gimzewski, J. K.; Aviram, A. Electronics Using Hybrid-Molecular and Mono-Molecular Devices. *Nature* **2000**, *408*, 541–548.
6. Green, J. E. Ultra-Dense Nano- and Molecular-Electronic Circuits. Ph.D. Dissertation, California Institute of Technology, Pasadena, CA, 2007.
7. Song, H.; Reed, M. A.; Lee, T. Single Molecule Electronic Devices. *Adv. Mater.* **2011**, *23*, 1583–1608.
8. Salomon, A.; Cahen, D.; Lindsay, S.; Tomfohr, J.; Engelkes, V. B.; Frisbie, C. D. Comparison of Electronic Transport Measurements on Organic Molecules. *Adv. Mater.* **2003**, *15*, 1881–1890.
9. Akkerman, H. B.; Blom, P. W. M.; de Leeuw, D. M.; de Boer, B. Towards Molecular Electronics with Large-Area Molecular Junctions. *Nature* **2006**, *441*, 69–72.
10. Zhou, C.; Deshpande, M. R.; Reed, M. A.; Jones, L.; Tour, J. M. Nanoscale Metal/Self-Assembled Monolayer/Metal Heterostructures. *Appl. Phys. Lett.* **1997**, *71*, 611–614.
11. Reed, M. A.; Zhou, C.; Muller, C. J.; Burgin, T. P.; Tour, J. M. Conductance of a Molecular Junction. *Science* **1997**, *278*, 252–254.
12. de Boer, B.; Frank, M. M.; Chabal, Y. J.; Jiang, W.; Garfunkel, E.; Bao, Z. Metallic Contact Formation for Molecular Electronics: Interactions between Vapor-Deposited Metals and Self-Assembled Monolayers of Conjugated Mono- and Dithiols. *Langmuir* **2004**, *20*, 1539–1542.
13. Lau, C. N.; Stewart, D. R.; Williams, R. S.; Bockrath, M. Direct Observation of Nanoscale Switching Centers in Metal/Molecule/Metal Structures. *Nano Lett.* **2004**, *4*, 569–572.
14. Preiner, M. J.; Melosh, N. A. Creating Large Area Molecular Electronic Junctions Using Atomic Layer Deposition. *Appl. Phys. Lett.* **2008**, *92*, 213301.
15. Shimizu, K. T.; Fabbri, J. D.; Jelincic, J. J; Melosh, N. A. Soft Deposition of Large-Area Metal Contacts for Molecular Electronics. *Adv. Mater.* **2006**, *18*, 1499–1504.
16. Gates, B. D.; Xu, Q.; Stewart, M.; Ryan, D.; Willson, C. G.; Whitesides, G. M. New Approaches to Nanofabrication: Molding, Printing and Other Techniques. *Chem. Rev.* **2005**, *105*, 1171–1196.
17. Wang, W.; Lee, T.; Reed, M. A. Mechanism of Electron Conduction in Self-Assembled Alkanethiol Monolayer Devices. *Phys. Rev. B* **2003**, *68*, 1–7.
18. Wang, W.; Lee, T.; Kretzschmar, I.; Reed, M. A. Comparison of Electronic Transport Characterization Methods for Alkanethiol Self-Assembled Monolayers. *Nano Lett.* **2004**, *4*, 643–646.
19. Kronemeijer, A. J.; Katsouras, I.; Huisman, E. H.; van Hal, P. A.; Geuns, T. C. T.; Blom, P. W. M.; de Leeuw, D. M. Universal Scaling of the Charge Transport in Large-Area Molecular Junctions. *Small* **2011**, *7*, 1593–1598.
20. Holmlin, R. E.; Haag, R.; Chabinyc, M. L.; Ismagilov, R. F.; Cohen, A. E.; Terfort, A.; Rampi, M. A.; Whitesides, G. M. Electron Transport through Thin Organic Films in Metal-Insulator-Metal Junctions Based on Self-Assembled Monolayers. *J. Am. Chem. Soc.* **2001**, *123*, 5075–5085.
21. Chiechi, R. C.; Weiss, E. A.; Dickey, M. D.; Whitesides, G. M. Eutectic Gallium-Indium (EGaIn): A Moldable Liquid Metal for Electrical Characterization of Self-Assembled Monolayers. *Angew. Chem., Int. Ed.* **2008**, *47*, 142–144.
22. Milani, F.; Grave, C.; Ferri, V.; Samori, P.; Rampi, M. A. Ultrathin π-Conjugated Polymer Films for Simple Fabrication of Large-Area Molecular Junctions. *ChemPhysChem* **2007**, *8*, 515–518.
23. Akkerman, H. B.; Kronemeijer, A. J.; van Hal, P. A.; de Leeuw, D. M.; Blom, P. W. M.; de Boer, B. Self-Assembled-Monolayer Formation of Long Alkanedithiols in Molecular Junctions. *Small* **2008**, *4*, 100–104.
24. Devaraj, N. K.; Decreau, R. A.; Ebina, W.; Collman, J. P.; Chidsey, C. E. D. Rate of Interfacial Electron Transfer through the 1,2,3-Triazole Linkage. *J. Phys. Chem. B* **2006**, *110*, 15955–15962.
25. Robinson, D. Kinetics of Electron Transfer through Organic Monolayers on Electrodes. Ph.D. Dissertation, Stanford University, Stanford, CA, 2002.
26. Wang, G.; Kim, Y.; Choe, M.; Kim, T.-W.; Lee, T. A New Approach for Molecular Electronic Junctions with a Multilayer Graphene Electrode. *Adv. Mater.* **2011**, *23*, 755–760.
27. Akkerman, H. Large Area Molecular Junctions. Ph.D. Dissertation, University of Groningen, The Netherlands, 2008.
28. Luebben, S.; Sapp, S. New Conducting and Semiconducting Polymers for Organic Photovoltaics *2010 MRS Spring Meeting*; San Francisco, CA, 2010.
29. Porter, M. D.; Bright, T. B.; Allara, D. L.; Chidsey, C. E. D. Spontaneously Organized Molecular Assemblies. 4. Structural Characterization of *n*-Alkyl Thiol Monolayers on Gold by Optical Ellipsometry, Infrared Spectroscopy, and Electrochemistry. *J. Am. Chem. Soc.* **1987**, *109*, 3559–3568.
30. Akkerman, H. B.; de Boer, B. Electrical Conduction through Single Molecules and Self-Assembled Monolayers. *J. Phys.: Condens. Matter* **2008**, *20*, 013001.
31. Engelkes, V. B.; Beebe, J. M.; Frisbie, C. D. Length-Dependent Transport in Molecular Junctions Based on SAMs of Alkanethiols and Alkanedithiols: Effect of Metal Work Function and Applied Bias on Tunneling Efficiency and Contact Resistance. *J. Am. Chem. Soc.* **2004**, *126*, 14287–14296.
32. McDermott, S.; George, C. B.; Fagas, G.; Greer, J. C.; Ratner, M. A. Tunnel Currents across Silane Diamines/Dithiols and Alkane Diamines/Dithiols: A Comparative Computational Study. *J. Phys. Chem. C* **2009**, *113*, 744–750.
33. Cheng, J.; Robinson, D. B.; Cicero, R. L.; Eberspacher, T.; Barrelet, C. J.; Chidsey, C. E. D. Distance Dependence of the Electron-Transfer Rate across Covalently Bound Monolayers. *J. Phys. Chem. B* **2001**, *105*, 10900–10904.
34. Cui, X. D.; Primak, A.; Zarate, X.; Tomfohr, J.; Sankey, O. F.; Moore, A. L.; Moore, T. A.; Gust, D.; Nagahara, L. A.; Lindsay, S. M. Changes in the Electronic Properties of a Molecule When It Is Wired into a Circuit. *J. Phys. Chem. B* **2002**, *106*, 8609–8614.
35. Morita, T.; Lindsay, S. Determination of Single Molecule Conductances of Alkanedithiols by Conducting-Atomic Force Microscopy with Large Gold Nanoparticles. *J. Am. Chem. Soc.* **2007**, *129*, 7262–7263.
36. Haiss, W.; Nichols, R. J.; van Zalinge, H.; Higgins, S. J.; Bethell, D.; Schiffrin, D. J. Measurement of Single Molecule Conductivity Using Spontaneous Formation of Molecular Wires. *Phys. Chem. Chem. Phys.* **2004**, *6*, 4330–4337.
37. van Hal, P. A.; Smits, E. C. P.; Geuns, T. C. T.; Akkerman, H. B.; De Brito, B. C.; Perissinotto, S.; Lanzani, G.; Kronemeijer, A. J.; Geskin, V.; Cornil, J.; *et al.* Upscaling, Integration and Electrical Characterisation of Molecular Junctions. *Nat. Nanotechnol.* **2008**, *3*, 749–754.
38. Weiss, E. A.; Chiechi, R. C.; Kaufman, G. K.; Kribel, J. K.; Zhefeng, L.; Duati, M.; Rampi, M. A.; Whitesides, G. M. Influence of Defects on the Electrical Characteristics of

Mercury-Drop Junctions: Self-Assembled Monolayers of *n*-Alkanethiolates on Rough and Smooth Silver. *J. Am. Chem. Soc.* **2007**, *129*, 4336–4349.
39. Simmons, J. G. Generalized Formula for the Electric Tunnel Effect between Similar Electrodes Separated by a Thin Insulating Film. *J. Appl. Phys.* **1963**, *34*, 1793–1803.
40. Simmons, J. G. Electric Tunnel Effect between Dissimilar Electrodes Separated by a Thin Insulating Film. *J. Appl. Phys.* **1963**, *34*, 2581–2590.
41. Simmons, J. G. Conduction in Thin Dielectric Films. *J. Phys. D: Appl. Phys.* **1971**, *4*, 613–657.
42. Li, X.; He, J.; Hihath, J.; Xu, B.; Lindsay, S. M.; Tao, N. Conductance of Single Alkanedithiols: Conduction Mechanism and Effect of Molecule-Electrode Contacts. *J. Am. Chem. Soc.* **2006**, *128*, 2135–2141.
43. Nardes, A. M. On the Conductivity of PEDOT:PSS Thin Films. Ph.D. Dissertation, Eindhoven University of Technology, Eindhoven, The Netherlands, 2007.
44. Li, L.; Meller, G.; Kosina, H. Temperature and Field-Dependence of Hopping Conduction in Organic Semiconductors. *Microelectron. J.* **2007**, *38*, 47–51.
45. Mandoc, M. M.; de Boer, B.; Paasch, G.; Blom, P. W. M. Trap-Limited Electron Transport in Disordered Semiconducting Polymers. *Phys. Rev. B* **2007**, *75*, 193202.
46. Montero, J.; Bisquert, J. Trap Origin of Field-Dependent Mobility of the Carrier Transport in Organic Layers. *Solid-State Electron.* **2011**, *55*, 1–4.
47. Gill, W. D. Drift Mobilities in Amorphous Charge-Transfer Complexes of Trinitrofluorenone and Poly-*n*-vinylcarbazole. *J. Appl. Phys.* **1972**, *43*, 5033–5040.
48. Unfortunately, we did not extensively measure SAM and polymer-only devices with the same pore diameter.
49. Mott, N. F. The Mobility Edge Since 1967. *J. Phys. C: Solid State Phys.* **1977**, *20*, 3075–3102.
50. Kronemeijer, A.; Huisman, E.; Katsouras, I.; van Hal, P.; Geuns, T.; Blom, P.; van der Molen, S.; de Leeuw, D. Universal Scaling in Highly Doped Conducting Polymer Films. *Phys. Rev. Lett.* **2010**, *105*, 156604.
51. Bockrath, M.; Cobden, D. H.; Lu, J.; Rinzler, A. G.; Smalley, R. E.; Balents, L.; McEuen, P. L. Luttinger-Liquid Behavior in Carbon Nanotubes. *Nature* **1999**, *397*, 598–601.
52. Yuen, J. D.; Menon, R.; Coates, N. E.; Namdas, E. B.; Cho, S.; Hannahs, S. T.; Moses, D.; Heeger, A. J. Nonlinear Transport in Semiconducting Polymers at High Carrier Densities. *Nat. Mater.* **2009**, *8*, 572–575.
53. Grabert, H.; Weiss, U. Quantum Tunneling Rates for Asymmetric Double-Well Systems with Ohmic Dissipation. *Phys. Rev. Lett.* **1985**, *54*, 1605–1608.
54. Fisher, M.; Dorsey, A. Dissipative Quantum Tunneling in a Biased Double-Well System at Finite Temperatures. *Phys. Rev. Lett.* **1985**, *54*, 1609–1612.
55. Neuhausen, A. Charge Transport in Molecular Junctions with Soft Contacts. Ph.D. Dissertation, Stanford University, Stanford, CA, 2012.
56. Schvartzman, M.; Wind, S. J. Robust Pattern Transfer of Nanoimprinted Features for Sub-5-nm Fabrication. *Nano Lett.* **2009**, *9*, 3629–3634.
57. Ron, H.; Matlis, S.; Rubinstein, I. Self-Assembled Monolayers on Oxidized Metals. 2. Gold Surface Oxidative Pretreatment, Monolayer Properties, and Depression Formation. *Langmuir* **1998**, *14*, 1116–1121.